Scientific Reports

https://doi.org/10.1038/s41598-026-61596-2

Article in Press

CaO-loaded cellulose acetate electrospun composite fibers: morphological, structural, and functional evaluation for biomedical applications

Received: 15 April 2026

Accepted: 6 July 2026

Published online: 13 July 2026

Cite this article as: Alkaron W., Tolnai I., Balázsi K. *et al.* CaO-loaded cellulose acetate electrospun composite fibers: morphological, structural, and functional evaluation for biomedical applications. *Sci Rep* (2026). https://doi.org/10.1038/s41598-026-61596-2

Wasan Alkaron, Istvan Tolnai, Katalin Balázsi & Csaba Balázsi

CaO-Loaded Cellulose Acetate Electrospun Composite Fibers: Morphological, Structural, and Functional Evaluation for Biomedical Applications

Wasan Alkaron[1,2, 3*], Istvan Tolnai[1*], Katalin Balázsi[1*] and Csaba Balázsi[1]

[1] Institute of Technical Physics and Materials Science, HUN-REN Centre for Energy Research, Konkoly-Thege, Miklós Str. 29-33, 1121 Budapest, Hungary

[2] Doctoral School of Materials Science and Technologies, Óbuda University, Bécsi Str. 96/B, 1030 Budapest, Hungary

[3] Technical Institute of Basra, Southern Technical University, Basra, Iraq

*Correspondence author email:
(W.A.) wasan.alkaron@ek.hun-ren.hu and (K.B.) balazsi.katalin@ek.hun-ren.hu

Abstract

This study presents a novel and sustainable approach for the fabrication of electrospun cellulose acetate (CA)/calcium oxide (CaO) composite fibers by utilizing bioactive CaO nanoparticles derived from calcined waste eggshells as an eco-friendly inorganic filler for advanced biomedical applications. CA/CaO composite solutions were prepared by mixing CaO powder of various proportions into a 10% CA solution and processed via electrospinning to produce composite fibers. The findings confirm the successful transformation of calcium carbonate ($CaCO_3$) into CaO through thermal calcination process. CaO particles were successfully incorporated into the fibers, with the median fiber diameter decreasing after CaO incorporation. Among the investigated samples, the CA/CaO composite fibers containing 2–6 wt% CaO showed the most favorable properties, providing a balance between fiber diameter, morphology, controlled and gradual calcium release in prepared phosphate-buffered saline (PBS), and chemical stability in prepared simulated body fluid solution (SPF).The hydrophilicity and water spreading behavior were

improved by the incorporation of CaO particles, as evidenced by the reduction in the contact angle to 60° compared with 81° for pure CA fibers. These results highlight an emerging method for producing novel biodegradable CA/CaO polymer composites with adjustable properties and enhanced hydrophilicity, providing a basis for future investigations of their suitability for biomedical applications.

Keywords: Electrospinning; Fibers composite; Hydrophilicity; Immersion test

Introduction

Scientists are increasingly focused on creating novel biomaterials for biomedical application through using natural and biowastes materials rather than expensive synthetic substances and dangerous chemicals [1–3]. These materials are designed to imitate natural systems by promoting cell adhesion, growth and specialization, and ensure compatibility with natural environment [4–6].

Electrospinning, a spinning technique, has been established as versatile and straightforward method to produce thin fibers from polymer solutions using electrostatic forces. Spun fibers offer several advantages such as an extremely high surface-to-volume ratio, tunable porosity, malleability to conform to a wide variety of sizes and shapes and the ability to control the nanofiber composition to achieve the desired results from its properties and functionality [7,8]. Electrospun fibers have been widely investigated in the past several years for their use across a wide range of areas, such as nanocatalysis, tissue engineering scaffolds, protective clothing, filtration, biomedical, pharmaceutical electronics, healthcare, biotechnology, defense and security, and environmental engineering [9,10]. In recent years, there has been an increasing interest in exploiting this technology to fabricate nanofibrous scaffolds that mimic the extracellular matrix and improve cellular infiltration, nutrition diffusion, and vascularization. Electrospun scaffolds from natural polymer materials possess several benefits, including

the ability to release antibiotics, bioactive minerals, and growth factors, thus enhancing osteogenesis, preventing infections, and facilitating tissue integration [11–14].

Despite encountering limitations of natural materials in mechanical strength and hydrophilicity, these challenges can be addressed through chemical modifications and surface treatments. Natural polymers such as cellulose acetate (CA) can be engineered to obtain structural support, making them promising candidates for repairing and bone regeneration [15,16].

The biological performance and bioactivity of electrospun CA scaffolds can be enhanced by fillers incorporated. Utilizing waste-derived fillers has emerged as an effective method to enhance polymer properties, offering an eco-friendly and cost-effective way to convert biowaste while also incorporating essential minerals into composite systems. Among these biowaste fillers, calcium oxide (CaO) derived from waste eggshells is particularly attractive as a bioactive ceramic additive due to its cost effective, biocompatibility, osteoconductivity, and capacity to stimulate bone regeneration. Waste eggshells are one type of agricultural waste that is released from food processing enterprises in large quantities, primarily consist of 94–97% calcium carbonate $CaCO_3$ can be easily converted into CaO through simple thermal treatment without the use of any chemical. This method can be considered a green synthesis and environmentally friendly route as no chemical reagent is used [17,18]. Incorporated CaO into polymer matrices promotes the formation of hydroxyapatite upon contact with physiological fluids, thus boosting the bioactivity of the scaffold. Furthermore, its alkaline properties enhance osteoblast attachment, growth, and differentiation. In addition to its antimicrobial activity, CaO also reduces the risk of infections in various wound settings, including those that are postoperative and chronic [19]. Integration of CaO into biodegradable polymers such as CA leads to enhancement of mechanical strength, regulate degradation rates, and improve surface wettability [20]. There are many attempts to develop biopolymer composites incorporating bioactive fillers for

biomedical applications [21–24]. For example, Canales et al. [25] developed novel electrospun scaffolds based on poly (lactic acid) PLA scaffolds reinforced with 10 and 20 wt% eggshell-derived CaO nanoparticles showed a significant improvement in mechanical properties of resultant composite. They demonstrated that the addition of CaO improved bioactivity by promoting hydroxyapatite formation and provided antibacterial activity. In this work, varying concentrations of CaO (2–10 wt%) were incorporated into a 10 wt% CA solution. The novelty of this study lies in the development of sustainable and biodegradable electrospun cellulose acetate/calcium oxide (CA/CaO) composite fibers utilizing CaO derived from waste eggshells as a low-cost and eco-friendly bioresource. Unlike conventional synthetic inorganic fillers, the present work demonstrates the successful conversion of waste eggshell-derived calcium carbonate into bioactive CaO through thermal calcination and its effective incorporation into electrospun CA fibers with homogeneous morphology and controlled fiber diameter. The addition of CaO particles enhanced both the hydrophilicity and the water spreading characteristics.

This work highlights a promising strategy for valorizing biowaste materials into high-value biomedical composites through electrospinning technology. Furthermore, the fabrication of these CA/CaO composites provides a platform for future investigations into the influence of CaO on the structural, thermal, and functional properties of composite materials. By tailoring their surface properties and structural integrity, these composites may be considered promising candidates for further evaluation in bone tissue engineering and other regenerative medicine applications.

Materials and methods

Materials

Cellulose acetate (CA, Mn = 30,000, 39.8% acetyl groups, Sigma Aldrich) employed as biopolymer matrices. Acetone (99.9% Fisher Chemical) Finland used as the solvent. All compounds were utilized as received, without any further purifying procedures. Distilled water was used throughout the entire experiment.

Preparation and synthesis of CaO from waste eggshells

Waste eggshells from chicken eggs were collected and rinsed multiple times with tap water to remove organic material and dried at room temperature. Then clean eggshells were crushed and milled in a ball mill and sieved with a mesh size of 40 µm to achieve sample uniformity. Finally, the resultant powder underwent thermal calcination in a furnace (DENKAL 4–K/1100, KALÓRIA Hőtechnikai Kft, Hungary) at 900 °C for 12 hours, enabling the transformation of $CaCO_3$ to CaO by thermal decomposition. The resultant powder cooled to ambient temperature and was stored in a sealed container to minimize moisture effects.

Preparation of CA/CaO solutions for electrospinning

Spinning solutions were prepared by dissolving CA powder in acetone at 10% and stirring at room temperature until a clear, homogeneous viscous solution was formed. Although acetone is a highly volatile solvent, it was selected due to its excellent solubility for cellulose acetate and its ability to promote rapid solvent evaporation during fiber formation. Consequently, CaO particles were added at varying concentrations of (0, 2, 4, 6, 8 and 10 wt%) to the 10% CA solution. The mixtures were prepared under continuous magnetic stirring to promote homogeneous dispersion within the polymer solution prior to electrospinning.

The prepared solution was subsequently loaded into a 10 mL plastic syringe and subjected to electrospinning using a standard vertical configuration (Electrospinning equipment model NE100 from Inovenso Electrospinning Co., Turkey). A stainless-steel needle with an internal diameter of 0.95 mm was connected to each syringe, and the solution was dispensed at a regulated flow rate with the help of a syringe pump. During electrospinning of pure CA solution a high voltage of 20 kV was applied between the needle and the aluminum foil-covered static collector, placed at a fixed distance of 12 cm from the needle tip with a flow rate of 1.0 mL/h. Whereas each composite solution was electrospun under optimized conditions of an applied voltage of 20 kV, a tip-to-collector distance of 10 cm, and flow rate of 1.5 mL/ h to

account for their higher viscosity. The electrospinning conditions were adjusted to achieve stable jet formation and continuous fiber production with minimal defects. All electrospinning experiments were carried out at ambient temperature and atmospheric pressure. The resulting fibrous mats of pure CA and composite fiber containing varying CaO contents, were used to investigate the effects of filler concentration on fiber morphology, structure, and potential functional properties.

Characterization methods

Scanning electron microscopy (SEM)

The morphological properties of raw eggshell powder, CaO powders, pure CA fibers, and CA/CaO composite fibers were examined using field-emission scanning electron microscopy (FE-SEM; Thermos Scientific Scios2, Waltham, MA, USA). The elemental composition and distribution were evaluated using Energy-Dispersive X-ray Spectroscopy (EDS; Oxford Instruments X-MaxN detector, Abingdon, UK).

Fourier transform infrared spectroscopy (FTIR)

Infrared spectroscopic investigation was performed using the attenuated total reflection (ATR) technique. A Varian Scimitar 2000 FT-IR spectrometer (Varian Inc., Palo Alto, CA, USA) equipped with an MCT (mercury–cadmium–telluride) detector was used and fitted with a ‘Golden Gate’ single reflection diamond ATR unit (Specac Ltd., Cray Ave, Orpington, UK). All spectra were collected with a nominal resolution of 4 cm^{-1} by the co-addition of 128 individual spectra. Before spectral evaluation, ATR correction was performed.

X-ray diffraction analysis (XRD)

CaO phases present in calcined eggshells and CA/CaO composite fibers were analyzed by X-ray diffraction (XRD; Bruker AXS D8 Discover, Karlsruhe, Germany), equipped with a Cu Kα radiation source (λ = 0.154 nm), a Göbel mirror, and a scintillation detector. The instrument was operated at 40 kV

and 40 mA. Phase identification and crystallographic analysis were carried out using Diffract Eva software (Bruker AXS).

Contact angle

The wettability of electrospun mats was evaluated through contact angle measurements. Distilled water was used as the test liquid. Approximately 2 µL of distilled water was dispensed onto each fiber mat for measurement. Five seconds after stabilization, droplet images were captured and analyzed using ImageJ software to measure the contact angle by marking points along the droplet. The software then computed a best-fitting tangent to calculate the contact angle perimeter [26]. Each measurement was repeated three times to ensure accuracy and reproducibility.

Leaching test

To evaluate the release of calcium ions, the fibers composite was immersed in prepared phosphate-buffered saline (PBS), which was prepared by dissolved reagent listed in (Table 1) in approximately 800 mL of distilled water, following the standard formulation [27–29]. The solution was stirred until complete dissolution, and the pH was adjusted to 7.4 at room temperature using 1 M HCl. The final volume was then adjusted to 1 L with distilled water. CA/CaO fibers composite containing 2, 4, 6, 8, and 10 wt% CaO were immersed in prepared PBS solutions for durations of 1, 7, and 14 days. At each interval, the fibers were removed and the solutions in which they were immersed were collected to determine the concentration of Ca ion. In addition, the pH of the immersion solution was measured at each time point using a calibrated digital pH meter to monitor alkalinity changes associated with CaO dissolution and ion release. The solutions were passed through a 0.45 µm syringe filter. Following filtration, the samples were acidified with concentrated HNO_3 and topped up to 10 mL by adding 8.9 mL distillated water and 0.1 mL of tested solution. Then, the samples diluted tenfold were analyzed using a PerkinElmer Avio 200 ICP-OES analytical methods at different time intervals.

Table (1) Composition of phosphate-buffered saline

Component	Amount (g/L)
NaCl	8.0
KCl	0.2
Na_2HPO_4	1.44
KH_2PO_4	0.24

Immersion test

Simulated body fluid (SBF) was prepared according to the Kokubo protocol to reproduce the ionic composition of human plasma [30]. The reagent (Table 2) sequentially dissolved in distilled water under continuous stirring at 36.5–37 °C, and the pH was adjusted to 7.40 at 37 °C using 1 M HCl. The solution was diluted to 1 L with distilled water and stored at 4 °C until use. CA/CaO fibers composite were immersed in SBF for 1, 7, and 14 days. The formation of calcium phosphate layers on the fiber surfaces was evaluated using SEM of the composite fibers in a simulated physiological environment.

Table (2) Composition of simulated body fluid (SBF)

Component	Amount (g)
NaCl	8.035
$NaHCO_3$	0.355
KCl	0.225
$K_2HPO_4 \cdot 3H_2O$	0.231
$MgCl_2 \cdot 6H_2O$	0.311
$CaCl_2$	0.292
Na_2SO_4	0.072
Tris	6.118

Results and discussion

Morphology and structure analysis of raw and calcinated eggshells

A morphological comparison of eggshell powder before and after calcining at 900 °C for 12 hours is shown in (Fig. 1a, and 1b). Uncalcined eggshell powder is characterized by irregular, angular particles with sharp edges and heterogeneous surface textures. The structure are generally dens compact have varying particle size, and agglomerate. Calcination modifies the morphology of eggshell particles, as illustrated in (Fig. 1b). The structure attains a granular and porous form, defined by uniform particle sizes and an

interlinked skeletal structure. The observed increase in surface area and roughness further confirms the thermal decomposition of $CaCO_3$ into CaO. The resultant morphology is consistent with earlier reports [31–33].

The elemental composition of the prepared CaO was confirmed using Energy-dispersive X-ray spectroscopy (EDS). The (EDS) displayed in (Fig. 1c) indicates phase change in calcinated eggshells which consist of calcium (Ca), oxygen (O), and small levels of magnesium (Mg) and sulfur (S) may represent residual contaminants inherently found in the raw eggshell matrix as illustrated in Table (3). These trace elements, for example Mg, have a significant impact on the promotion of osteogenesis and angiogenesis by acting as one of the positively charged substitutes for calcium in the calcium phosphate structure [34].

Table (3) Element composition of raw and calcined eggshell

Element	Raw eggshell weight%	Calcined eggshell weight%
C	31.39	12.24
O	48.09	56.09
Ca	18.45	30.88
Mg	0.23	0.58
N	1.31	-----
P	0.09	trace
S	0.37	0.08
Na	0.09	trace

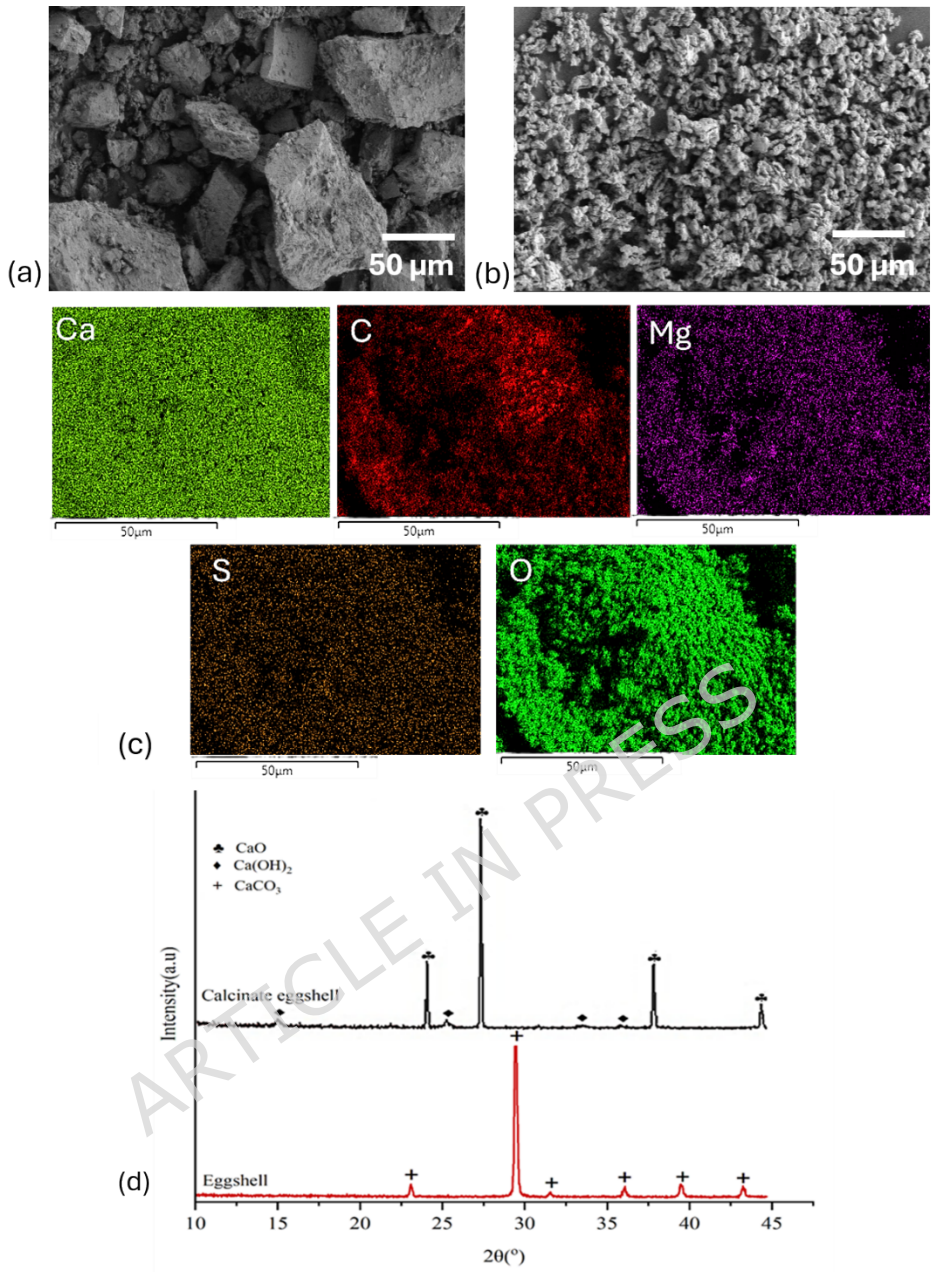

Fig. 1. Surface morphology of (a) untreated eggshell and (b) treated eggshell powder subjected to a temperature of 900°C for 12 hours (c) EDS elemental maps of treated eggshell powder (d) XRD patterns for untreated and thermally treated eggshells.

Furthermore, the XRD analysis verifies the successful conversion of calcite-based eggshells into CaO (JCPD 01-082-1690). The XRD pattern of the untreated eggshell clearly revealed $CaCO_3$ in its calcite crystalline form, with characteristic diffraction peaks at $2\theta \approx 23°$, 29.4°, 36°, 39°, 43°, and 47°. These peaks clearly indicate that raw eggshells mainly consist of crystalline

$CaCO_3$ with small amorphous content or secondary phases. Calcination induced phase transformation in the diffraction pattern. The primary constituents of calcined eggshells are CaO and calcium hydroxide ($Ca(OH)_2$) (JCPD 00-044-1481). The presence of CaO peaks at $2\theta \approx 23°$, 27°, 37°, and 45° suggests that $CaCO_3$ has been efficiently decomposed to CaO through thermal treatment [35]. It is thought that $Ca(OH)_2$ is produced due to the partial hydration of CaO when it is managed or encounters the moisture in the air following calcination [17]. Based on the observed morphological changes, elemental profile and XRD analysis, it is evidence that the chosen calcination parameters (900 °C for 12 h) effectively decompose $CaCO_3$ to high-purity CaO [35].

Morphology analysis of CA/CaO composite fibers

The characteristics of CaO derived from eggshell waste by calcination render particles suitable for reinforcing the fiber structure of pure CA, as they possess increased surface area, porosity, and regularity in structure.

The effect of CaO incorporation on fiber uniformity, diameter, and structural integrity is clearly observable in (Fig. 2). At CaO concentrations of 2%, 4%, and 6%, the SEM of those groups showed uniform dispersion and distribution of CaO particles within the fiber matrix without evident agglomeration or structural defects. The CaO particles were well-dispersed, and their small size did not disrupt the electrospinning process, allowing for the formation of continuous, well-formed fibers despite the minor increase in surface roughness. SEM analysis, therefore, confirmed the successful fabrication of uniform CA/CaO composite fibers with CaO loadings of 2–6 wt.%, demonstrating that the selected solvent system and processing conditions were effective for achieving adequate particle dispersion and stable electrospinning. A study by Münchow et al.[36] showed that the fibers preserved their structural integrity when electrospun from polymer matrices containing low concentration s of the incorporated filler.

At a CaO loading of 8%, significant morphological changes were observed. Although the fiber network remains mostly intact, there is an increase in surface irregularities, and clear signs of CaO particles clustering on or within the fiber surfaces, as highlighted by the red box. Localized bulges and defects are formed by these accumulations, disrupting fiber continuity. An electrospinning process with 10% CaO loading becomes highly unstable, as evidenced by the SEM image displaying extensive beading, fiber coalescence, and large CaO agglomerates. Red arrows pinpoint major sites where CaO has accumulated and caused structural deformation. This high loading effect on the viscosity of the polymer solution and the stability of the electrospinning jet, resulting in fiber fusion and particle sedimentation [37]. The resulting nonuniform fiber networks, exhibit bead formation, and show signs of precipitation of CaO particles.

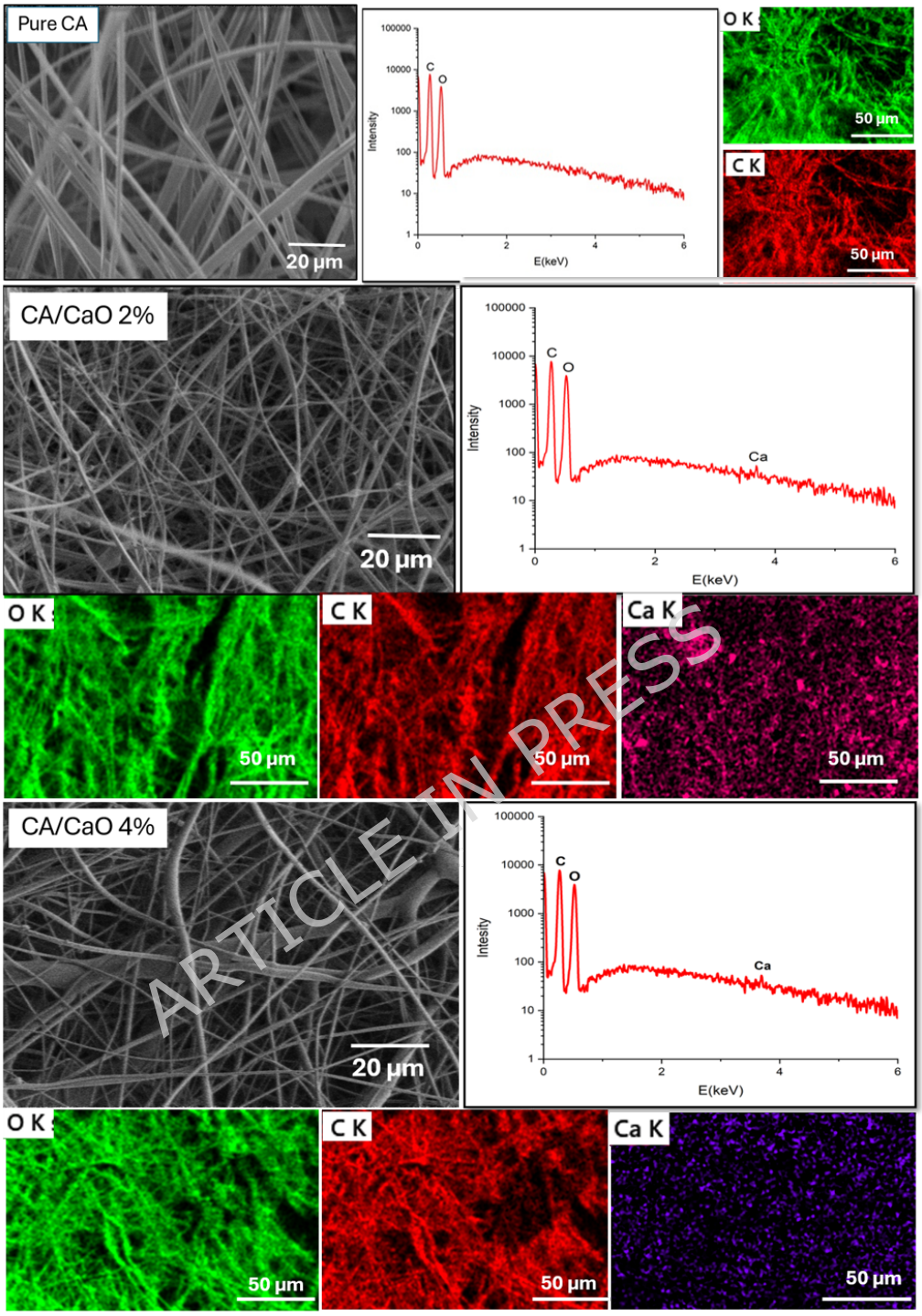

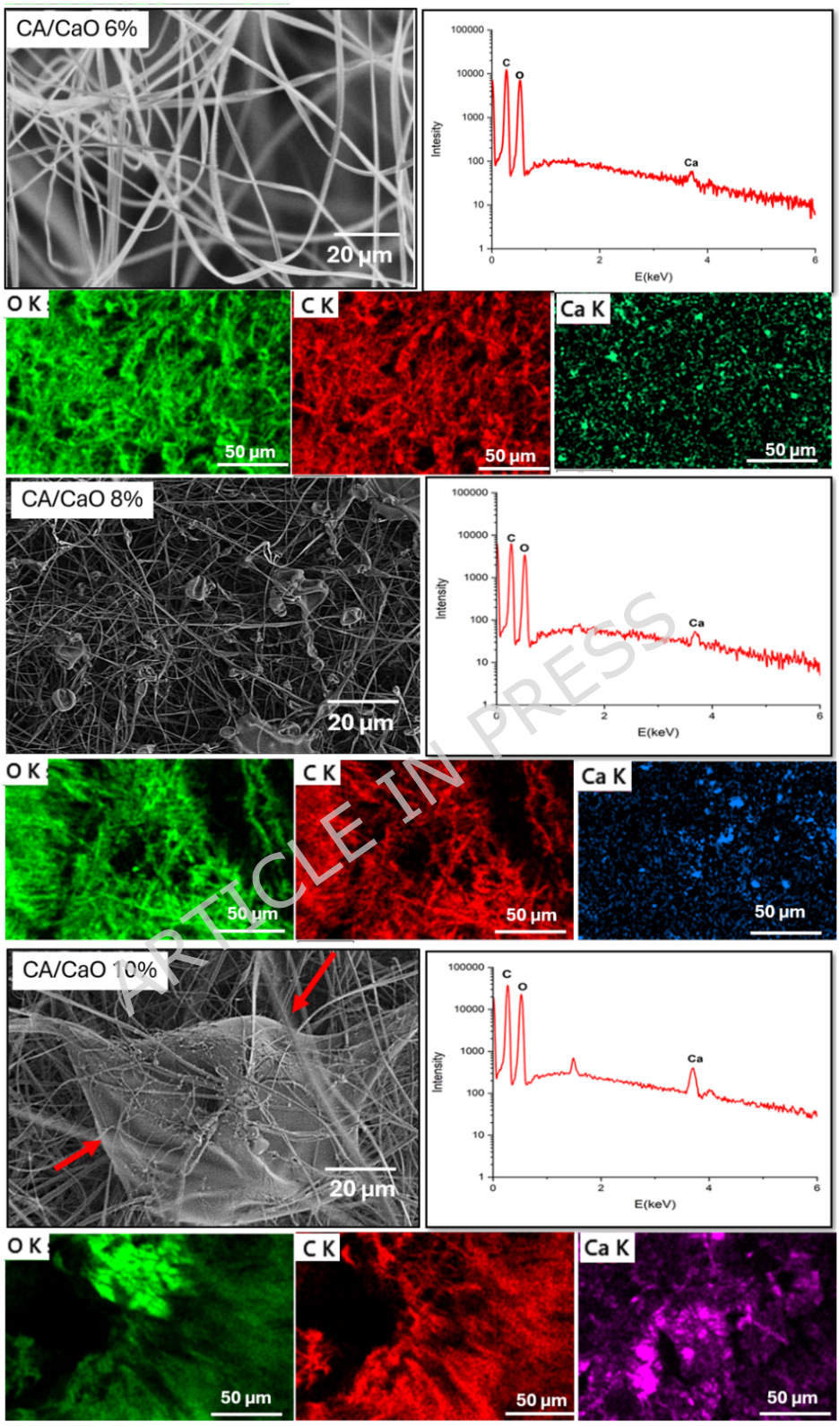

Fig. 2. SEM and EDS analysis of pure CA fibers and CA/CaO composite fibers with different loadings of CaO concentration 2%, 4%, 6%, 8%, and 10%.

The EDS analysis clearly illustrates the effective integration of CaO into the CA matrix, as shown in (Fig. 2). The EDS show only C and O peaks in pure CA, while a weak Ca signal emerges at 2% CaO. From 4% onward, Ca peaks become well defined and intensify as loading increases, the inorganic phase is effectively integrated and evenly distributed within the polymer matrix. This indicates that at higher concentrations, CaO not only exists but also becomes increasingly prominent in the composite structure.

The influence of CaO incorporation on the diameter of electrospun CA fibers is presented in (Fig. 3). A clear trend was observed that increasing CaO content results in a progressive reduction in fiber diameter. Pure CA fibers (Fig. 3a) display a broad diameter distribution, with a mean of 875 nm, which falls within the range of values reported in the literature [38,39]. A stable jet generally promotes the formation of continuous fibers with moderate uniformity. The incorporation of CaO results in a marked reduction in fiber diameter. At a load of just 2% CaO, the average fiber diameter decreases to 687 nm (Fig. 3b). The decreasing trend continues with CaO additions, which reaches 526 nm at 4% and 330 nm at 6%. The gradual decrease in fiber diameter with increasing CaO content may be attributed to the increased electrical conductivity of the electrospinning solution caused by CaO particles. Higher conductivity enhances electrostatic stretching of the polymer jet during electrospinning, resulting in thinner fibers. Additionally, the dispersion of CaO particles may affect polymer chain interactions and jet stretching behavior, further influencing fiber formation.[40,41].

A mean fiber diameter of 277 nm has been determined at 8% CaO loading, suggesting that this concentration may be close optimal for producing ultrafine and uniform fibers. However, as shown in the SEM images (Fig. 2), the onset of CaO particle accumulation within the fiber matrix becomes apparent at this stage. Although the reduction in diameter is desirable, this localized accumulation may slightly affect the surface morphology and overall fiber uniformity.

In the case of CaO loading of 10%, the mean fiber diameter is reduced to 153 nm. However, this significant reduction is accompanied by notable structural drawbacks. Morphological irregularities such as beading, fiber merging, and CaO clustering, become more pronounced. The excessive particles seem to destabilize the electrospinning jet, causing inconsistencies in the process [42]. This instability promotes localized accumulation of CaO, reduces effective polymer concentration, and results in the formation of ultrafine fibers that are structurally weakened.

It can be concluded from these results that the range of (2-6) % CaO loaded fibers offer best balance between the diameter and quality of the fibers.

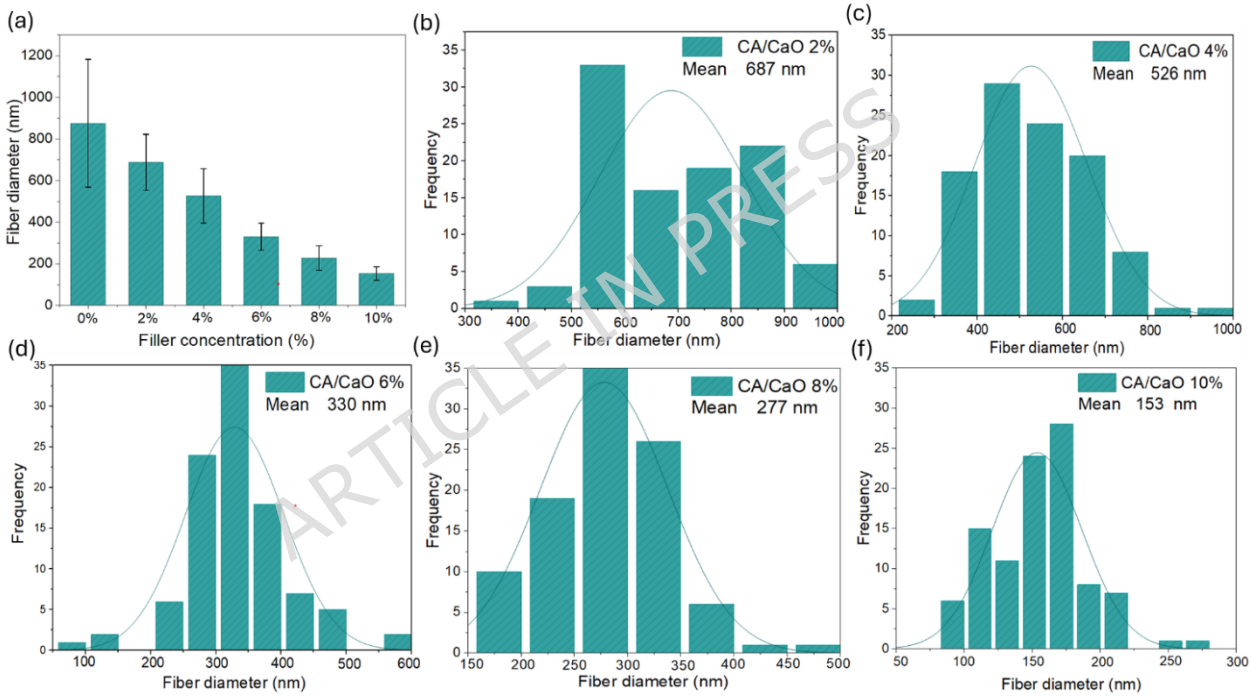

Fig. 3. (a) Variation trend of average fiber diameter with filler concentration, based on measurements of no fewer than 100 fibers per condition, error bars represent standard deviation. (b)–(f) average fiber diameters and corresponding diameter distribution histograms of CA/CaO nanofibers with varying CaO (b) 2 wt%, (c) 4 wt%, (d) 6 wt%, (e) 8 wt%, and (f) 10 wt%.

FTIR and XRD analysis of CA and CA/CaO composite fibers

Fig. 4 (a) presents the FTIR spectra of pure CA, CaO, and CA/CaO composite fibers. The spectrum of pure CA exhibit a broad O–H stretching vibration

around 3480 cm^{-1}, a C–H stretching vibration around 2940 cm^{-1}, and strong C=O stretching absorption from the ester group near 1740 cm^{-1} as well as C–O–C stretching bands around 1230 to 1020 cm^{-1} [43].

The FTIR spectrum of CaO displays two broad absorption bands in the range of 1000–1500 cm^{-1}, which is attributed to Ca–O lattice vibrations. This suggests the successful transformation from $CaCO_3$ to CaO [44,45]. In addition, CaO exhibits a small and sharp absorption peak at around ~3700 cm^{-1} which is attributed to the surface-adsorbed O–H groups, from minor hydration or atmospheric moisture [46].

The spectra are evidently changed when CaO is incorporated into the CA matrix. Observations indicate a decrease in O-H stretching band intensity at 3480 cm^{-1} with the addition of CaO.

The observed effect may arise from an interaction between the CA and CaO hydroxyl groups, or there may be fall in the quantity of free hydroxyl groups. There was partial crosslinking between the polymer matrix and inorganic filler, as supported by these data [36].

However, new absorption bands are observed in the 3750 cm^{-1} (as indicated by black arrow). These features are characteristic of O-H band and suggest that CaO particles are effectively integrated and well-dispersed into the polymer matrix. The intensity of CaO-associated bands progressively increases with increasing CaO content, especially for the 8 wt% and 10 wt% composites, confirming the increasing presence of the inorganic phase. Importantly, no significant shifts were observed in the principal CA backbone peaks indicating that the incorporation of CaO did not alter the fundamental chemical structure of the polymer matrix. These findings collectively confirm the successful fabrication of CA/CaO composite fibers with effective interfacial interactions between the organic and inorganic components.

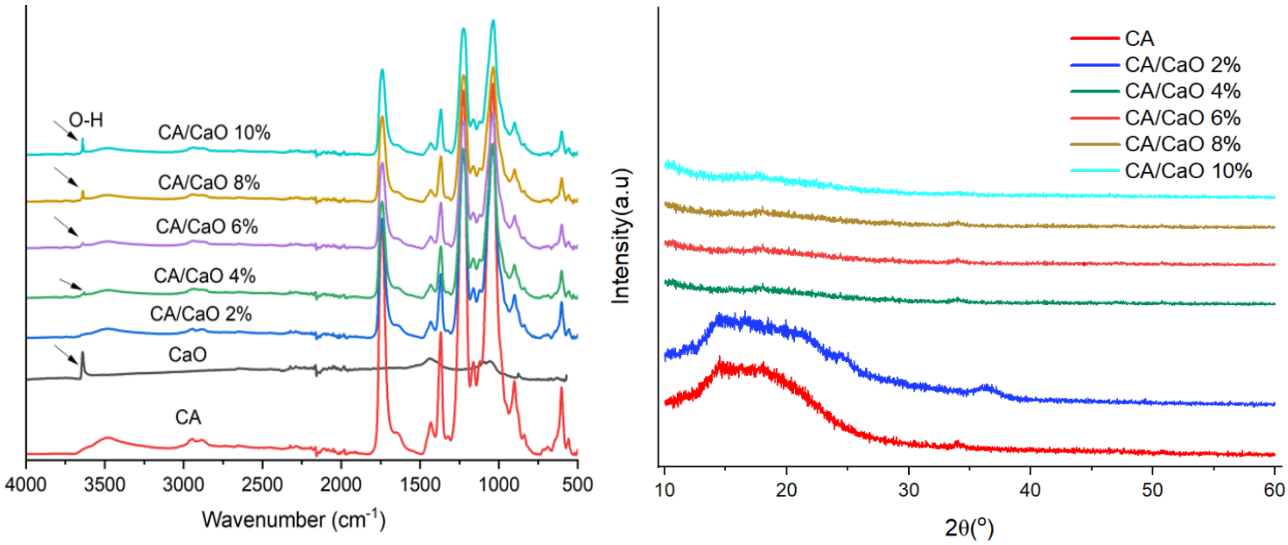

Fig. 4. (a) FTIR spectra and (b) XRD patterns of CA and CA/CaO fiber composite at different CaO loading.

Fig. 4 (b) illustrates the findings from X-ray diffraction studies, which were performed to assess how the phase composition of CA fibers changes as the CaO content varies between 2 and 10 wt%. Pure CA exhibits a broad amorphous halo centered at approximately 2θ = 20°, which is characteristic of the predominantly amorphous structure of cellulose acetate. Similar observations have been reported in previous studies [47, 48].

Upon incorporation of CaO, the intensity of this broad halo gradually diminished with increasing filler content, consistent with either a dilution of the amorphous CA domains or a disruption caused by well-dispersed CaO particles. Interestingly, the composite spectra do not display any distinct crystalline peaks typical of CaO, which is probably due to the dispersion or the naturally low crystallinity of the CaO phase within the polymer matrix. The general flattening of the diffraction curves at higher CaO concentrations indicates that the inclusion of CaO suppresses any potential semi-crystalline ordering in CA, which might also influence the material's mechanical characteristics. These XRD analysis provide strong confirmation of the

successful incorporation of CaO and its direct impact on the microstructure of the CA fibers, aligning well with observations from FTIR spectroscopy.

Contact angle

The wettability and hydrophilicity of electrospun fibers are a crucial parameter that directly impacts cell adhesion and growth in tissue engineering application [49] [50]. The water contact angle is a widely used parameter for assessing the hydrophilicity or hydrophobicity of droplet over the fibrous mats. (Fig. 5 a, b) shows the image of droplets to assess the water contact angle of pure CA and CA/CaO fibrous composite materials. The pure CA fiber demonstrated a notably hydrophilic surface ($\theta = 81°$), which can be attributed to the abundance of hydroxyl groups on the polymer's surface [51]. However, the incorporation of CaO into the CA fiber polymer matrix led to a steady and noticeable decrease in contact angle values. The water contact angles drop from 77° at 2 wt% to 62° at 10 wt%, in comparison to the pure fibers. This effect can be attributed to the inherent characteristics of CaO, and the presence of hydroxyl groups readily form on CaO surface when interact with moisture, allowing more hydrophilic sites for water affinity. Moreover, the decrease in fiber diameter with increasing CaO content, as observed in the SEM analysis of composite fibers, indirectly reinforces this effect by increasing surface roughness, which, together with the presence of hydrophilic CaO particles, further enhances the overall wettability of the composite surface. This trend indicates that CaO is an effective modifier for tuning the surface characteristics of CA fibers, offering interesting strategies to enhance hydrophilicity through compositional adjustment [36, 50].

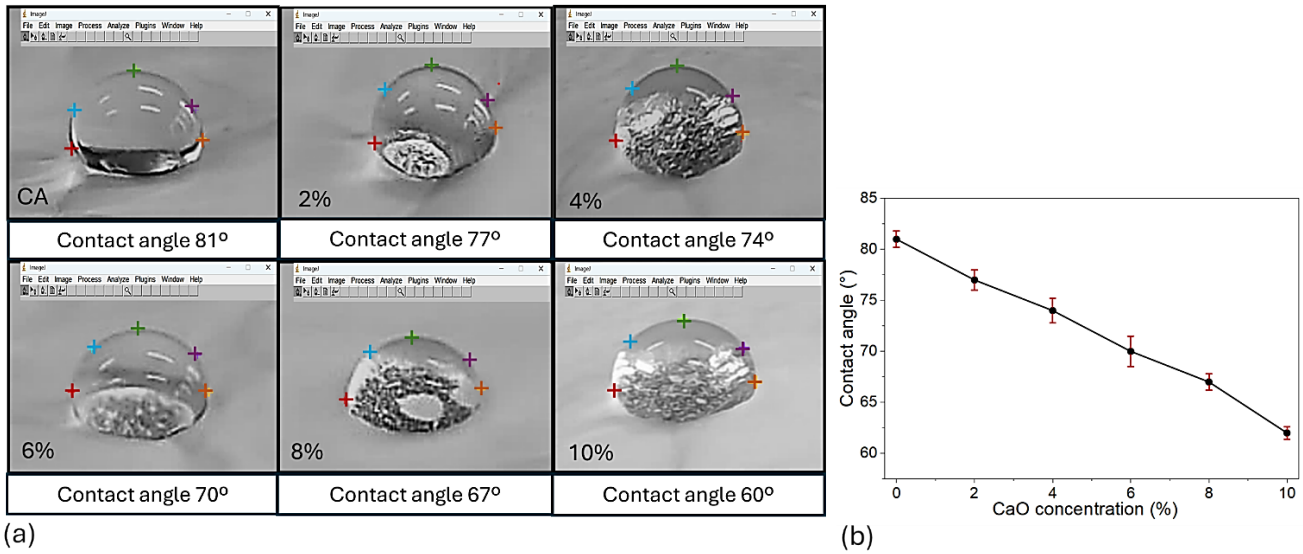

Fig. 5. Contact angle measurements of CA and CA/CaO composite fibers at different CaO concentrations (a) images of droplet analyzed by image J software (b) inset plot of contact angle values against CaO concentration.

Calcium ion release

The presence of calcium ions (Ca^{2+}) in the surrounding environment plays a crucial role in the mineralization process of bone graft materials [52,53]. (Fig. 6) presents the cumulative Ca^{2+} release from fibers containing different CA/CaO compositions (2%, 4%, 6%, 8%, and 10%) after 1, 7, and 14 days of immersion in PBS, as determined by ICP analysis.

In all compositions, the release of Ca^{2+} ions increased as the immersion time extended

over the 14-day measurement period, indicating a continuous leaching of ions into the PBS solution. This release pattern, which depends on time, implies that the process is mainly controlled by the initial dissolution of CaO on the surface, followed by the diffusion of Ca^{2+} ions into the surrounding environment. The results are consistent with previous study [54,55]

The samples with 2%, 4%, and 6% concentrations demonstrated moderate and regulated calcium release patterns. This controlled release of ions is beneficial for biomedical uses, as it aids in maintaining ionic balance in

physiological settings and minimizes abrupt changes in local solution chemistry[56].

In comparison, the 8% and 10% samples showed significantly higher Ca^{2+} release throughout the immersion period. Excessive calcium leaching may lead to increased alkalinity of the surrounding medium due to hydroxyl ion formation, which may undermine material stability and adversely affect biological responses. Therefore, although higher Ca^{2+} release may enhance mineralization potential, uncontrolled ion release is generally undesirable for practical bone tissue engineering applications[57].

The leaching results are consistent with the previously observed fiber morphology. Fiber composite with 8% and 10% CaO exhibits poor fiber quality, as indicated by formation of beads and significant agglomeration of CaO particles (Fig. 2). It is likely that these structural irregularities lead to localized dissolution and increased ion release and higher leaching behavior. In contrast, the 2%, 4%, and 6% samples show a more consistent fiber morphology, leading to a more controlled and gradual calcium release. Therefore, these fibers composite further investigated to analysis their bioactivity in SBF solution.

The pH evolution of the CA/CaO composite fibers showed in Table (4). The pH of the CA/CaO composite fibers initially increased with increasing CaO content due to the hydration and dissolution of CaO, which released Ca^{2+} and OH^- ions into the medium. At day 7, the pH remained elevated, indicating continued ion release and enhanced alkalinity, particularly for higher CaO loadings. By day 14, a gradual decrease in pH was observed in all samples, which can be attributed to the consumption of OH^- ions during calcium-phosphate mineral deposition and continued ion exchange between the composite fibers and the surrounding medium, which gradually shifts the pH toward more moderate values.

Table 4. pH values of CA/CaO composite fibers after immersion in PBS for 1, 7, and 14 days.

Composites	Day 1	Day 7	Day 14
CA/CaO 2%	7.5	8.0	7.7
CA/CaO 4%	8.0	8.3	8.0
CA/CaO 6%	8.4	8.6	8.1
CA/CaO 8%	9.4	9.6	9.1
CA/CaO 10%	10.5	11.1	10.2

The composites with 2–6 wt% CaO exhibited a moderate and stable pH range, suggesting controlled ion release and favorable bioactivity, whereas the 8–10 wt% CaO composites generated higher alkalinity due to accelerated CaO dissolution. These results indicate that 2–6 wt% CaO provides a better balance between calcium release, pH stability, and potential biomedical performance.

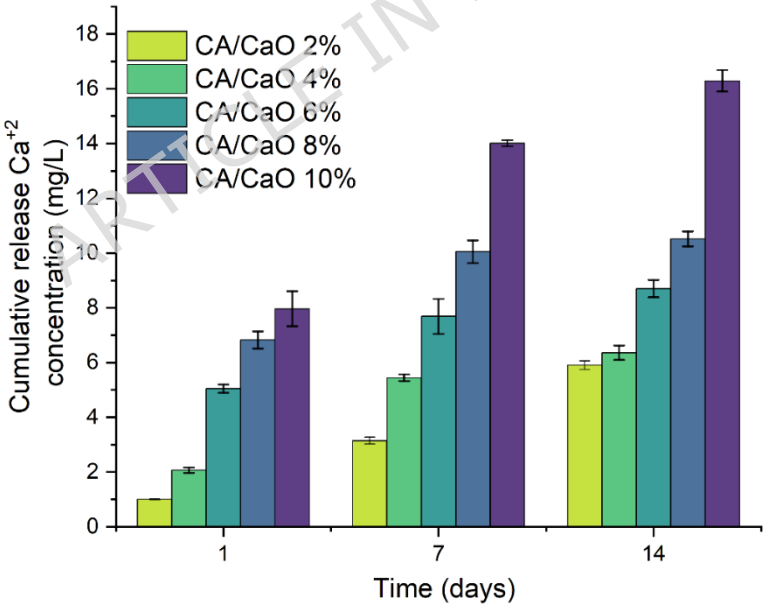

Fig. 6. Calcium ion releases from different composite fibers after (1, 7, and 14) days immersing in the PBS solution.

Immersion analysis

The behavior of the CA/CaO composite fibers containing 2%, 4%, and 6% CaO were examined by soaking the samples in prepared SBF solution for 1, 7, and 14 days. Distinct morphological differences are observed among these compositions, demonstrating that CaO content significantly influences. Moreover, calcium phosphate-containing deposits formation was enhanced during the period of immersion in SBF as shown in (Fig. 7a).

For the 2% and 4% CaO composite fibers depict uniform layers of fine particulate deposits visible on the surfaces. These deposits look like sparsely distributed and exhibit small granular or plate-like morphologies after one day of exposure to SBF. This suggests a moderate and sustained release of Ca^{2+} ions, sufficient to induce surface-mediated calcium phosphate formation without promoting excessive precipitation or structural degradation.

In the 6% CaO composite fiber, the SEM images demonstrate that the bioactivity specimen had a denser arrangement of apatite crystals. The fiber surfaces are more extensively covered with deposited particles, forming semi-continuous coatings in several regions. The deposits show plate-like and agglomerated features, reflecting enhanced calcium phosphate formation compared to the lower CaO contents. After 7 and 14 days of immersing in SBF, the irregular crystal structure of the apatite formed due to multiple crystal growth and the transformation of calcium phosphate was faster in all examined specimens.

It can be concluded that fiber compositions (2-6) % appear to provide a favorable balance between calcium ion release and controlled apatite formation while retaining morphological integrity.

The elemental maps (Fig.7 b) indicate the presence of (C) and (O) from the CA polymer matrix, as well as (Ca) and phosphorus (P), confirming the formation of calcium-phosphate deposits in the fiber composite after immersion in SBF. The relatively even spatial distribution of Ca and P throughout the examined areas indicates a uniform deposition of calcium phosphate phases on the fiber surfaces.

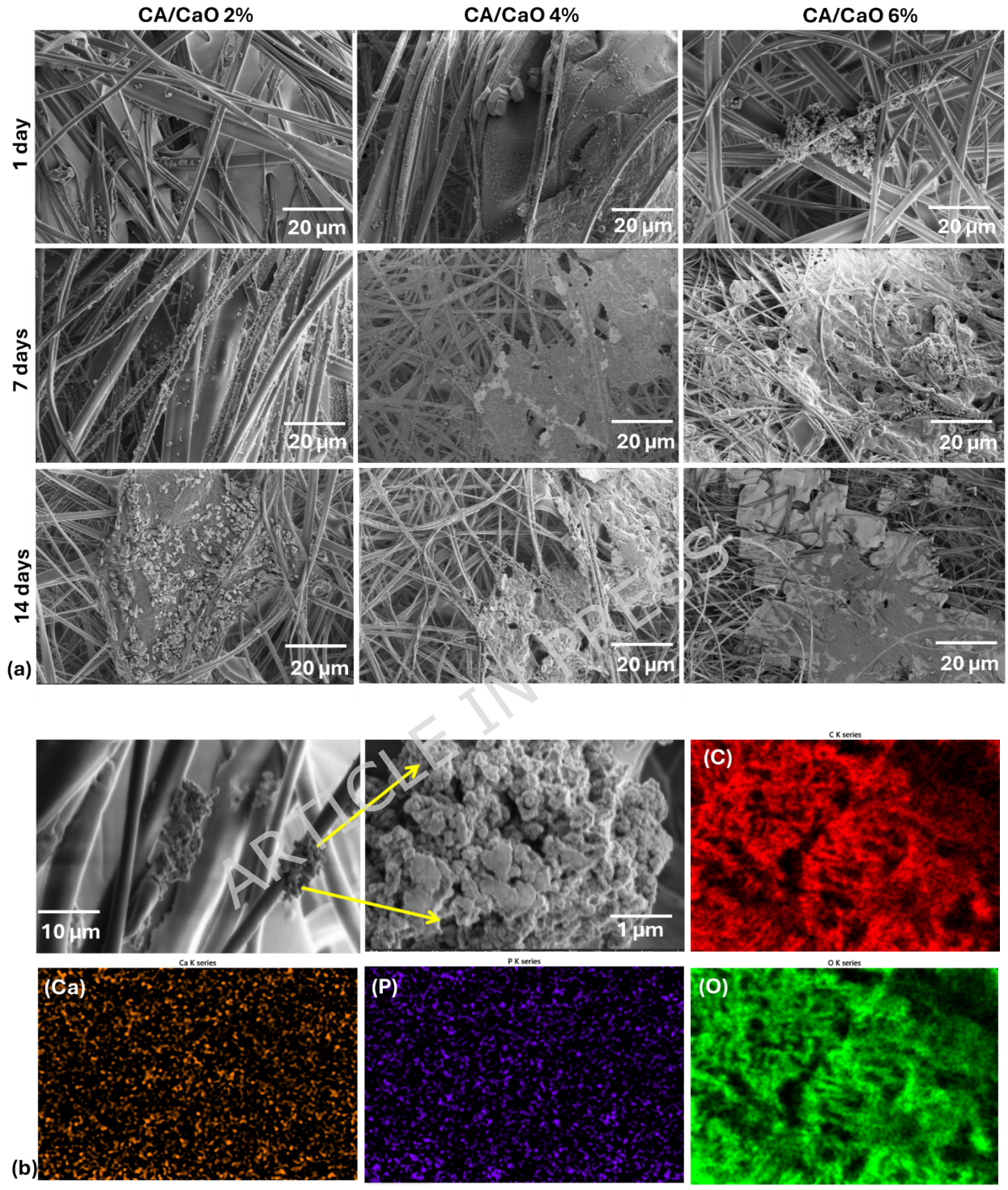

Fig. (7) (a) SEM images of composite fibers containing 2%, 4%, and 6% CaO after immersion in SBF solution for up to 14 days (b) SEM of selected

composite fibers at low and high magnification and their compositional mapping after immersed in SPF solution.

Conclusion

This study demonstrated the successful conversion of waste eggshells into CaO through thermal calcination and its incorporation into electrospun CA fibers. The addition of CaO significantly influenced the electrospinning process, fiber morphology, wettability, ion-release behavior, and bioactivity of the resulting composites. While increasing CaO content reduced fiber diameter due to enhanced solution conductivity and electrostatic stretching, excessive loadings (8–10 wt%) promoted particle agglomeration, impaired spinnability, and deteriorated fiber quality.

FTIR and XRD analyses confirmed the successful incorporation of CaO into the CA matrix, whereas contact angle measurements revealed enhanced hydrophilicity with increasing CaO content. Calcium-release, pH, and SBF immersion studies demonstrated that composites containing 2–6 wt% CaO exhibited controlled ion release, moderate alkalinity, favorable mineralization behavior, and good structural stability. In contrast, higher CaO loading resulted in excessive calcium release, stronger alkalinity, and reduced morphological integrity.

Although the 6 wt% sample showed relatively denser mineral deposition. The results demonstrated that the 2–6 wt% CaO composition was identified as the most suitable range, providing the best balance of fiber uniformity, electrospinnability, controlled Ca^{2+} release, moderate pH, improved hydrophilicity, and favorable mineralization behavior. In addition, this composition range was easier to prepare and process by electrospinning compared with higher CaO loadings (8–10 wt%), which exhibited poorer spinnability due to increased particle loading and agglomeration. These findings highlight the potential of converting agro-industrial waste into functional and eco-friendly CA/CaO composite fibers while supporting sustainable circular economy strategies. The obtained physicochemical

properties suggest that these materials may be suitable candidates for future biomedical investigations. Although the present study provides valuable insights into the morphological and physicochemical properties of the CA/CaO composite fibers, additional investigations are required to fully assess their performance. Future studies should include comprehensive mechanical and thermal characterization, together with in vitro cytocompatibility, antibacterial, and in vivo evaluations to verify the functionality, safety, and potential biomedical applicability of the developed composites.

Acknowledgement

The authors sincerely thank colleagues from HUN-REN Centre for Energy Research, Viktor Varga and Balázs Erki for their assistance in preparation samples, Dr. Z. E. Horváth for technical assistance with the XRD analysis, Tamás Kolonits for help in SEM/EDS characterization and Dr. Kornél Fél for technical assistance with the FTIR analysis of the samples. The paper is partially supported by Southern Technical University under scientific research awards, No. 9/7934,10 Sep. 2025.

Data availability

Data will be available from the corresponding author upon request.

Competing interests

The authors declare no conflict of interest.

Funding

The project presented in this article is supported by the National Research, Development, and Innovation Office—OTKA NKFI 146076.

References

1. Selim, M., Mousa, H. M., Abdel-Jaber, G. T., Barhoum, A. & Abdal-hay, A. Innovative designs of 3D scaffolds for bone tissue regeneration:

Understanding principles and addressing challenges. *Eur. Polym. J.* **215**, 113251 (2024).

2. Alkaron, W., Almansoori, A., Balázsi, K. & Balázsi, C. Hydroxyapatite-Based Natural Biopolymer Composite for Tissue Regeneration. *Materials* **17**, 4117 (2024).

3. Reddy, M. S. B., Ponnamma, D., Choudhary, R. & Sadasivuni, K. K. A Comparative Review of Natural and Synthetic Biopolymer Composite Scaffolds. *Polymers (Basel).* **13**, 1105 (2021).

4. Bolamperti, S., Villa, I. & Rubinacci, A. Bone remodeling: an operational process ensuring survival and bone mechanical competence. *Bone Res.* **10**, 48 (2022).

5. Jain, T. *et al.* RETRACTED: Biomimetic Materials for Regenerative Medicine: Design and Applications. *E3S Web of Conferences* **505**, 04002 (2024).

6. Biglari, N. *et al.* Advanced biomaterials in immune modulation: The future of regenerative therapies. *Int. J. Pharm.* 125972 (2025) doi:10.1016/j.ijpharm.2025.125972.

7. Ahmadi Bonakdar, M. & Rodrigue, D. Electrospinning: Processes, Structures, and Materials. *Macromol* **4**, 58–103 (2024).

8. Zaarour, B., Zhu, L. & Jin, X. Direct fabrication of electrospun branched nanofibers with tiny diameters for oil absorption. *J. Dispers. Sci. Technol.* **42**, 2085–2091 (2021).

9. Gupta, K. C., Haider, A., Choi, Y. & Kang, I. Nanofibrous scaffolds in biomedical applications. *Biomater. Res.* **18**, (2014).

10. Zhu, L., Zaarour, B. & Jin, X. Fabrication of perfect CMCS/PVA nanofibers for keeping food fresh via an *in situ* mixing electrospinning. *Mater. Res. Express* **6**, 125001 (2019).

11. Suamte, L. & Babu, P. J. Electrospun based functional scaffolds for biomedical engineering: A review. *Nano TransMed* 100055 (2024) doi:10.1016/j.ntm.2024.100055.

12. Alkaron, W., Almansoori, A., Balázsi, C. & Balázsi, K. A Critical Review of Natural and Synthetic Polymer-Based Biological Apatite Composites for Bone Tissue Engineering. *Journal of Composites Science* **8**, 523 (2024).

13. Gouma, P., Xue, R., Goldbeck, C. P., Perrotta, P. & Balázsi, C. Nano-hydroxyapatite—Cellulose acetate composites for growing of bone cells. *Materials Science and Engineering: C* **32**, 607–612 (2012).

14. Balázsi, K. *et al.* Biogenic Nanosized Hydroxyapatite for Tissue Engineering Applications. in 190–193 (2013). doi:10.1007/978-3-642-34197-7_50.

15. Zhang, Y., Zhang, C. & Wang, Y. Recent progress in cellulose-based electrospun nanofibers as multifunctional materials. *Nanoscale Adv.* **3**, 6040–6047 (2021).

16. Konwarh, R., Karak, N. & Misra, M. Electrospun cellulose acetate nanofibers: The present status and gamut of biotechnological applications. *Biotechnol. Adv.* **31**, 421–437 (2013).

17. Tangboriboon, N., Kunanuruksapong, R. & Sirivat, A. Preparation and properties of calcium oxide from eggshells via calcination. *Materials Science-Poland* **30**, 313–322 (2012).

18. Alkaron, W. A., Hamad, S. F. & Sabri, M. M. Studying the Fabrication and Characterization of Polymer Composites Reinforced with Waste Eggshell Powder. *Advances in Polymer Technology* **2023**, 1–9 (2023).

19. Ielo, I., Calabrese, G., De Luca, G. & Conoci, S. Recent Advances in Hydroxyapatite-Based Biocomposites for Bone Tissue Regeneration in Orthopedics. *Int. J. Mol. Sci.* **23**, 9721 (2022).

20. Min, K. H., Kim, D. H., Kim, K. H., Seo, J.-H. & Pack, S. P. Biomimetic Scaffolds of Calcium-Based Materials for Bone Regeneration. *Biomimetics* **9**, 511 (2024).

21. Al-Harbi, N. *et al.* Bioactive hybrid membrane-based cellulose acetate/bioactive glass/hydroxyapatite/carbon nanotubes nanocomposite for dental applications. *J. Mech. Behav. Biomed. Mater.* **141**, 105795 (2023).

22. Jayakrishnan, A., Shahana, S. & Ayswaria, R. Preparation and evaluation of bioactive cellulose acetate films from *Musa acuminata*. *RSC Sustainability* **2**, 2335–2347 (2024).

23. Ramanathan, G. *et al.* Fabrication of Biohybrid Cellulose Acetate-Collagen Bilayer Matrices as Nanofibrous Spongy Dressing Material for Wound-Healing Application. *Biomacromolecules* **21**, 2512–2524 (2020).

24. Almansoori, A. & Alkaron, W. Effect of low-pressure plasma treatment on the thermal behaviour of organo-modified montmorillonite nanoclay. *Archives of Materials Science and Engineering* **125**, 5–14 (2024).

25. Canales, D. *et al.* Preparation and characterization of novel poly (lactic acid)/calcium oxide nanocomposites by electrospinning as a potential bone tissue scaffold. *Biomaterials Advances* **153**, 213578 (2023).

26. W. S., R. ,National Institutes of Health 'Image Processing and Analysis in Java Program, (ImageJ 1.x)', [computer program] Available at: http://imagej.nih.gov/ij.

27. Schille, C. *et al.* Corrosion of experimental magnesium alloys in blood and PBS: A gravimetric and microscopic evaluation. in *Materials Science and Engineering: B* vol. 176 1797–1801 (Elsevier Ltd, 2011).

28. Alvarez-Lopez, M. *et al.* Corrosion behaviour of AZ31 magnesium alloy with different grain sizes in simulated biological fluids. *Acta Biomater.* **6**, 1763–1771 (2010).

29. Xue, D., Yun, Y., Tan, Z., Dong, Z. & Schulz, M. J. *In Vivo and In Vitro Degradation Behavior of Magnesium Alloys as Biomaterials*. *J. Mater. Sci. Technol* vol. 28 (2012).

30. Kokubo, T. & Takadama, H. How useful is SBF in predicting in vivo bone bioactivity? *Biomaterials* **27**, 2907–2915 (2006).

31. Supriyanto, N. S. W., Sukarni, Puspitasari, P. & Permanasari, A. A. Synthesis and characterization of CaO/CaCO3 from quail eggshell waste by solid state reaction process. in 040032 (2019). doi:10.1063/1.5115670.

32. Marques Correia, L., Cecilia, J. A., Rodríguez-Castellón, E., Cavalcante, C. L. & Vieira, R. S. Relevance of the Physicochemical Properties of Calcined Quail Eggshell (CaO) as a Catalyst for Biodiesel Production. *J. Chem.* **2017**, 1–12 (2017).

33. Ahmad, W., Sethupathi, S., Munusamy, Y. & Kanthasamy, R. Valorization of Raw and Calcined Chicken Eggshell for Sulfur Dioxide and Hydrogen Sulfide Removal at Low Temperature. *Catalysts* **11**, 295 (2021).

34. Bharadwaj, A. V. S. L. S., Singh, M., Niju, S., Begum, K. M. M. S. & Anantharaman, N. Biodiesel production from rubber seed oil using

calcium oxide derived from eggshell as catalyst – optimization and modeling studies. *Green Processing and Synthesis* **8**, 430–442 (2019).

35. Rahmayanti, M., Fatimah, I., Yahdiyani Ikhsani, A. & Nur Azizah, D. The potential of calcium oxide nanocatalyst from chicken eggshells for biodiesel production using chicken fat waste. *Inorg. Chem. Commun.* **165**, 112604 (2024).

36. Münchow, E. A. *et al.* Synthesis and characterization of CaO-loaded electrospun matrices for bone tissue engineering. *Clin. Oral Investig.* **20**, 1921–1933 (2016).

37. Gonzalez, E., Barquero, A., Muñoz-Sanchez, B., Paulis, M. & Leiza, J. R. Green Electrospinning of Polymer Latexes: A Systematic Study of the Effect of Latex Properties on Fiber Morphology. *Nanomaterials* **11**, 706 (2021).

38. Sinha, R., Janaswamy, S. & Prasad, A. Enhancing Mechanical Properties of Electrospun Cellulose Acetate Fibers Upon Potassium Chloride Exposure. *SSRN Electronic Journal* https://doi.org/10.2139/ssrn.3604714 (2020) doi:10.2139/ssrn.3604714.

39. Kakoria, A. & Sinha-Ray, S. A Review on Biopolymer-Based Fibers via Electrospinning and Solution Blowing and Their Applications. *Fibers* **6**, 45 (2018).

40. Schofield, R. M. *et al.* Driving fiber diameters to the limit: nanoparticle-induced diameter reductions in electrospun photoactive composite nanofibers for organic photovoltaics. *Adv. Compos. Hybrid Mater.* **6**, 229 (2023).

41. Bachs-Herrera, A., Yousefzade, O., del Valle, L. J. & Puiggali, J. Melt Electrospinning of Polymers: Blends, Nanocomposites, Additives and Applications. *Applied Sciences* **11**, 1808 (2021).

42. Cho, Y. *et al.* Electrospinning and Nanofiber Technology: Fundamentals, Innovations, and Applications. *Advanced Materials* **37**, (2025).

43. Chen, J., Xu, J., Wang, K., Cao, X. & Sun, R. Cellulose acetate fibers prepared from different raw materials with rapid synthesis method. *Carbohydr. Polym.* **137**, 685–692 (2016).

44. Joshi, G. *et al.* Transesterification of Jatropha and Karanja oils by using waste egg shell derived calcium based mixed metal oxides. *Energy Convers. Manag.* **96**, 258–267 (2015).

45. Ahmad, W., Sethupathi, S., Munusamy, Y. & Kanthasamy, R. Valorization of Raw and Calcined Chicken Eggshell for Sulfur Dioxide and Hydrogen Sulfide Removal at Low Temperature. *Catalysts* **11**, 295 (2021).

46. Rasool, T. *et al.* Synthesis and Characterization of Hydroxyapatite Using Egg-Shell. in *Volume 3: Biomedical and Biotechnology Engineering* (American Society of Mechanical Engineers, 2015). doi:10.1115/IMECE2015-51933.

47. Candido, R. G., Godoy, G. G. & Gonçalves, A. R. Characterization and application of cellulose acetate synthesized from sugarcane bagasse. *Carbohydr. Polym.* **167**, 280–289 (2017).

48. Phan, D.-N. *et al.* Investigation of Mechanical, Chemical, and Antibacterial Properties of Electrospun Cellulose-Based Scaffolds Containing Orange Essential Oil and Silver Nanoparticles. *Polymers (Basel).* **14**, 85 (2021).

49. Alsulaiman, L. *et al.* Synthesis and Characterization of Cellulose Acetate—HBA/Poly Sulfone Blend for Water Treatment Applications. *Membranes (Basel).* **15**, 38 (2025).

50. García, G. *et al.* Electrospun scaffolds based on a PCL/starch blend reinforced with CaO nanoparticles for bone tissue engineering. *Int. J. Biol. Macromol.* **273**, 132891 (2024).

51. Röhrl, M. *et al.* New Functional Polymer Materials via Click Chemistry-Based Modification of Cellulose Acetate. *ACS Omega* **8**, 9889–9895 (2023).

52. Chang, Y.-L., Stanford, C. M. & Keller, J. C. Calcium and phosphate supplementation promotes bone cell mineralization: Implications for hydroxyapatite (HA)-enhanced bone formation. *J. Biomed. Mater. Res.* **52**, 270–278 (2000).

53. An, S., Gao, Y., Ling, J., Wei, X. & Xiao, Y. Calcium ions promote osteogenic differentiation and mineralization of human dental pulp cells: implications for pulp capping materials. *J. Mater. Sci. Mater. Med.* **23**, 789–795 (2012).

54. Seol, Y.-J. *et al.* Improvement of Bone Regeneration Capability of Ceramic Scaffolds by Accelerated Release of Their Calcium Ions. *Tissue Eng. Part A* **20**, 2840–2849 (2014).

55. Le, T. D. H., Tuan, H. N. A., Nguyen, V. T. & Le, A. T. Hydroxyapatite−loaded starch/polyvinyl alcohol scaffold for bone regeneration application: preparation and characterization. *J. Solgel Sci. Technol.* **107**, 441–451 (2023).

56. Subramaniam, T., Fauzi, M. B., Lokanathan, Y. & Law, J. X. The Role of Calcium in Wound Healing. *Int. J. Mol. Sci.* **22**, 6486 (2021).

57. Retegi-Carrión, S., Ferrandez-Montero, A., Eguiluz, A., Ferrari, B. & Abarrategi, A. The Effect of Ca2+ and Mg2+ Ions Loaded at Degradable PLA Membranes on the Proliferation and Osteoinduction of MSCs. *Polymers (Basel).* **14**, 2422 (2022).